energies

MDPI

Article

Performance of a Solar Thermoelectric Power-Harvesting Device Based on an All-Glass Solar Heat Transfer Pipe and Gravity-Assisted Heat Pipe with Recycling Air Cooling and Water Cooling Circuits

Zhe Zhang, Yafeng Wu, Wenbin Li * and Daochun Xu *

Key Lab of State Forestry Administration on Forestry Equipment and Automation, School of Technology, Beijing Forestry University, Beijing 100083, China; zhangzhe8562@gmail.com (Z.Z.); xdl_wyf314@163.com (Y.W.)

* Correspondence: leewb@bjfu.edu.cn (W.L.); xudaochun@bjfu.edu.cn (D.X.); Tel.: +86-010-6233-8139 (W.L.); +86-136-8146-2745 (D.X.)

Received: 20 December 2019; Accepted: 17 February 2020; Published: 20 February 2020

Abstract: For the purpose of collecting solar radiation for energy conversion and utilization and improving the output performance of thermoelectric power-generation components, a new solar thermoelectric conversion device based on an all-glass solar heat transfer pipe and gravity-assisted heat pipe with recycling air cooling and water cooling circuits is designed. The uniqueness of the device lies in the combination of gravity-assisted heat pipes with excellent thermal conductivity and a direct air-cooled mode, a fin-cooled mode, and two solar-driven water-cooling modes with different flow rates. Based on the structure, the device can realize four separate output modes and multiple composite output modes and has practical significance for meeting different load power requirements, such as wireless sensors and electronics. Under a state of regular illumination from 3.14×10^4 lx to 10.04×10^4 lx, with one thermoelectric power generator (TEG) in one mode, the peak output voltage and power values of the device in single-output mode range from 183.1 mV to 370.7 mV and 33.5 mW to 137.2 mW, respectively, proving the feasibility of the proposed device. The energy supply of the above structure is completely obtained from the natural environment, and this aspect provides a high reference value for the cross-research of natural environment energy utilization and thermoelectric energy-conversion technology.

Keywords: solar energy; thermoelectric; cooling; thermodynamics

1. Introduction

Thermoelectric technology has become a popular means of energy conversion in recent years because of the rapid development of thermoelectric materials [1,2]. Thermoelectric materials provide a reliable source of heat transfer between two or more electromagnets, and thermoelectric power generators are a research hotspot in thermodynamics. Benefitting from light weight, high reliability, low cost, lack of noise, and environmental friendliness, an increasing number of thermoelectric power generators have been investigated, analysed and widely used to solve power supply limitation issues.

Due to the low energy efficiency of thermoelectric materials, the output power of thermoelectric power devices is limited, which greatly hinders the promotion and utilization of thermoelectric technology. To obtain a higher output power, more researchers have begun to combine thermoelectric power with solar energy. As a result, solar thermoelectric power generation and photovoltaic and thermoelectric power generation (PV/TEG) systems have attracted the attention of researchers. Zhang Z et al. presented a thermoelectric power-generation system that absorbed solar power and supplied power for low-power loads [3]. Later, a solar thermoelectric power-generation system was developed

by Zhang Z et al. and achieved a larger output with the application of heat transfer pipes [4]. Demir ME et al. designed a solar thermoelectric power-generation system that is beneficial for fresh water production [5]. Karthick K et al. achieved 24 h of continuous work by a solar thermoelectric power generator through an energy storage method [6]. Kumar A et al. studied the temperatures of various areas of a solar pond to improve the output of thermoelectric power generation [7]. Sathiyanathan M et al. discussed the output parameters of a solar thermoelectric power energy converter [8]. The excellent behaviour of a solar thermoelectric generator was demonstrated by Zhang XF et al. [9]. Zhu W et al. presented a thin-film solar thermoelectric generator that is suitable for sensor applications [10]. Furthermore, Kwan TH et al. demonstrated the advantages of a PV/TEG system over conventional thermoelectric power generation [11]. A hybrid PV/TEG system with a cavity designed by Marandi OF et al. achieved three times the amount of power generated by ordinary PV/TEG systems [12]. Singh S et al. evaluated a concentrated PV-TEG system to provide a reference for related studies [13]. Lekbir A et al. discussed the viability and advantages of a PV-TEG system when applied in energy-harvesting fields [14]. Zhu W et al. realized a better output with a PV-TEG system than with ordinary PV units through the optimization of thermal structures [15].

With the help of energy-conversion technology, thermoelectric material advancement and photovoltaic science, thermoelectric power generators have been widely applied in environmental energy-harvesting fields, especially in supplying power to various loads. However, several limitations remain to be solved. As a limitation of thermoelectric materials, the thermoelectric power conversion efficiency is far from satisfactory. Furthermore, the temperature difference between the hot side and cold side of thermoelectric power generators is still not large and stable, and this limitation deserves further study. On this point, studies of the heating or cooling methods of thermoelectric power generators have become significant. In fact, studies of the heating methods of thermoelectric power generators have become a focus of recent thermoelectric research, and various heating methods, such as the concentration of solar energy, choice of high-temperature streams and use of other fuels as heating sources, have been discussed. According to the Seebeck effect, the temperature of the cold side of a thermocouple is closely related to the cooling effect of the cold end. Therefore, studying the cooling effect of the cold end of a thermocouple is significant for the development of cooling research. Karimov KS et al. presented a two-stage solar thermoelectric power generator cooled by outdoor air with a glass lens [16]. Rodrigo PM et al. established a model of a PV-TEG system, choosing air cooling as its cooling method [17]. Maolikul S et al. studied the behaviour of the battery of a thermoelectric power generator whose cooling method was outdoor air cooling [18]. Chen WH et al. chose an indoor water-cooling method to demonstrate the benefits of improving the output performance of a thermoelectric power generation system [19]. Ding LC et al. compared the performance of an outdoor pump-powered water-cooled thermoelectric system with that of solar ponds [20]. Ma M et al. analysed the cooling parameters of a thermoelectric power generator equipped with an indoor water-cooling structure [21]. Date A et al. discussed the performance of a system including a solar heating structure and TEG, whose cooling method was indoor water cooling [22].

In this article, for the purpose of improving the output performance of a thermoelectric power-generation process, a new solar thermoelectric conversion device based on an all-glass solar heat transfer pipe and gravity-assisted heat pipe with recycling air cooling and water cooling circuits is designed. The distinguishing feature of the device is the combination of gravity-assisted heat pipes with excellent thermal conductivity and a direct air-cooled mode, a fin-cooled cooling mode, and two solar-driven water-cooling modes with different flow rates. The output performance of four different cooling modes located on the cold sides of the thermocouples of the thermoelectric power-generation device is continuously tested and measured in natural outdoor circumstances. Two series of experiments are designed to test the output parameters of the system. The first series of experiments studied the performance of the output current, output voltage of the load resistance, output power and thermoelectric efficiency of the thermoelectric module with a large-channel water cooling radiator in the case of a gradual increase in load resistance when the temperatures of the hot and

cold sides of the thermoelectric module vary within relatively stable small ranges. The second series of experiments concentrated on the continuous working status of thermoelectric modules with four different cooling modes, where the output parameters of the four different cooling modes are discussed and analysed to provide a reference for related continuous working cooling research. The results clearly show the cooling effects of four cooling structures located on the cold side of the thermocouples of the thermoelectric power-generation device. With different cooling media, including water, aluminium and air, the device provides data support for a single application or combinations of cooling modes in different cooling circumstances. Based on the structure mentioned above, the device is capable of matching the complex requirements of wireless sensors, electronic modules, and other similar loads. More importantly, the energy supply of the above structure is completely obtained from the natural environment, and this aspect provides a high reference value for the cross-research of natural environment energy utilization and thermoelectric energy-conversion technology.

2. Materials and Methods

During the energy-collection process of the concentrated solar thermoelectric power-generation device, solar energy is absorbed and transferred to the conductive copper block through an all-glass solar heat transfer pipe and a gravity-assisted heat pipe. The energy that reaches the conductive copper block can be expressed as follows:

$$Q_{block} = Q_{absorb} - Q_{rad,gl} = A_S q_S \alpha_{ab.gr} - (A_S q_S \alpha_{ab.gl} - Q_{cvn,gl} - Q_{rad,gl-loss}) \quad (1)$$

$$Q_{rad,gl} = A_S q_S (\alpha_{ab.gl-out} + \alpha_{ab.gl-in}) - Q_{cvn,gl-out} - Q_{cvn,gl-in} - Q_{rad,gl-loss} \quad (2)$$

$$Q_{cvn,gl} = Q_{cvn,gl-out} + Q_{cvn,gl-in} = h_{gl}(T_{gl-out} - T_{Evi}) + h_{gl}(T_{gl-in} - T_{air}) \quad (3)$$

$$Q_{rad,gl-loss} = \varepsilon_{gl}\sigma(T_{gl-out}^4 - T_{Evi}^4) \quad (4)$$

$$Q_{block} = A_S q_S \alpha_{ab.gr} - A_S q_S (\alpha_{ab.gl-out} + \alpha_{ab.gl-in}) + h_{gl}(T_{gl-out} + T_{gl-in} - T_{air} - T_{Evi}) + \varepsilon_{gl}\sigma(T_{gl-out}^4 - T_{Evi}^4) \quad (5)$$

where Q_{absorb} is the entire amount of solar energy absorbed by the solar thermoelectric power-generation device; $Q_{rad,gl}$ and $Q_{rad,gl-loss}$ are the energy radiation in the energy-collection process from the all-glass solar heat transfer pipe to the environment and the energy loss of the aforementioned process caused by the outer part of the all-glass solar heat transfer pipe, respectively; q_S is the solar energy per unit area; A_S is the area of solar energy collection; $\alpha_{ab,gr}$, $\alpha_{ab,gl}$, $\alpha_{ab,gl-in}$ and $\alpha_{ab,gl-out}$ represent the absorption by the gravity-assisted heat pipe, all-glass solar heat transfer pipe, and the inner part and outer part of the all-glass solar heat-transfer pipe of the solar thermoelectric device, respectively; $Q_{cvn,gl}$, $Q_{cvn,gl-in}$ and $Q_{cvn,gl-out}$ represent the solar energy lost from the all-glass solar heat-transfer pipe and the inner part and outer part of the all-glass solar heat transfer pipe to the surroundings by convection, respectively; h_{gl} is the convection coefficient of the all-glass solar heat-transfer pipe during the energy-collection process; and ε_{gl}, σ, T_{air} and T_{Evi} are the average surface emissivity of the all-glass solar heat-transfer pipe, the Stefan-Boltzmann constant, the air temperature in the inner part of the all-glass solar heat transfer pipe device surface, and the temperature of the environment surrounding the outer part of the all-glass solar heat-transfer pipe device surface, respectively.

The energy that reaches the conductive copper block can be conducted as the energy source of the hot sides of the four thermoelectric modules attached tightly to the surface of the conductive copper block, and these modules are equipped with four different cooling structures. Here,

$$Q_{block} = Q_{bwh} + Q_{swh} + Q_{alh} + Q_{airh} \quad (6)$$

$$Q_{bwh} = \alpha_{teg} I_{bw} T_{bwh} + K_{TE}\Delta T_{bw} - \frac{1}{2} R_{TE} I_{bw}^2 \quad (7)$$

$$Q_{swh} = \alpha_{teg} I_{sw} T_{swh} + K_{TE}\Delta T_{sw} - \frac{1}{2} R_{TE} I_{sw}^2 \quad (8)$$

$$Q_{alh} = \alpha_{teg} I_{al} T_{alh} + K_{TE} \Delta T_{al} - \frac{1}{2} R_{TE} I_{al}^2 \tag{9}$$

$$Q_{airh} = \alpha_{teg} I_{air} T_{airh} + K_{TE} \Delta T_{air} - \frac{1}{2} R_{TE} I_{air}^2 \tag{10}$$

where Q_{bwh}, Q_{swh}, Q_{alh} and Q_{airh} are the energy that reaches the hot side of the thermoelectric module with a large-channel water cooling radiator, a small-channel water cooling radiator, an aluminium air cooling radiator and direct air cooling, respectively. The energy that reaches the hot side of the thermoelectric module is converted into electric power or transferred by the cooling structure. Then,

$$Q_{bwc} = \frac{S_{teg} N_u K_{fluid} (T_{bwc} - T_{fluid-bw})}{d_{channel-bw}} = \alpha_{teg} I_{bw} T_{bwc} + K_{TE} \Delta T_{bw} - \frac{1}{2} R_{TE} I_{bw}^2 \tag{11}$$

$$Q_{swc} = \frac{S_{teg} N_u K_{fluid} (T_{swc} - T_{fluid-sw})}{d_{channel-sw}} = \alpha_{teg} I_{sw} T_{swc} + K_{TE} \Delta T_{sw} - \frac{1}{2} R_{TE} I_{sw}^2 \tag{12}$$

$$Q_{alc} = \frac{(T_{alc} - T_{flow-al})}{R_{thermal,al} + R_{thermal,teg}} = \alpha_{teg} I_{al} T_{alc} + K_{TE} \Delta T_{al} - \frac{1}{2} R_{TE} I_{al}^2 \tag{13}$$

$$R_{thermal,al} = \frac{H_{al}}{K_{al} S_{cross-al}} + \frac{\mu_{flow}^{-1/5} \cdot \mathrm{Pr}^{2/3}}{0.037 (\rho_{flow} L_{al})^{-1/5} C_P u_{flow}^{4/5} S_{al}} \tag{14}$$

$$Q_{airc} = \frac{(T_{ac} - T_{flow})}{R_{thermal,teg}} = \alpha_{teg} I_{air} T_{ac} + K_{TE} \Delta T_{air} - \frac{1}{2} R_{TE} I_{air}^2 \tag{15}$$

where Q_{bwc}, Q_{swc}, Q_{alc}, and Q_{ac} are the energy acquired at the cold side of the thermoelectric module with a large-channel water cooling radiator, a small-channel water cooling radiator, an aluminium air cooling radiator and a direct air cooling structure, respectively; α_{teg} and S_{teg} are the Seebeck coefficient and the area of the thermoelectric power generator, respectively; N_u is the Nusselt number; K_{fluid} is the thermal conductivity of the cooling fluid; $d_{channel-bw}$ and $d_{channel-sw}$ are the diameters of the large channel and small channel, respectively; T_{bwc}, T_{swc}, $T_{fluid-bw}$, $T_{fluid-sw}$, ΔT_{bw}, and ΔT_{sw} are the temperature of the cold side, temperature of the cooling fluid, and temperature difference between the hot and cold sides of the thermoelectric module with a large-channel water cooling radiator and a small-channel water cooling radiator, respectively; H_{al}, K_{al} and $S_{cross-al}$ are the height, thermal conductivity and cross-section area of the aluminium radiator, respectively; u_{flow}, ρ_{flow} and μ_{flow} are the velocity, density and viscosity coefficient of the air flow, respectively; Pr is the Prandtl number; C_P is the heat capacity of air; L_{al} and S_{al} are the length and whole area of the aluminium radiator, respectively; $R_{thermal,al}$ and $R_{thermal,teg}$ are the thermal resistances of the aluminium air-cooling radiator and TEG, respectively; and T_{alc}, T_{ac}, $T_{flow-al}$, T_{flow}, ΔT_{al}, and ΔT_{air} are the temperature of the cold side, the temperature of the air flow, and the temperature difference between the hot and cold sides of the thermoelectric module with an aluminium air-cooling radiator and a direct air cooling structure, respectively.

The whole output power of the concentrated solar thermoelectric power generation system can be calculated as follows:

$$P_{OUT} = P_{BW} + P_{SW} + P_{AL} + P_{AIR} = Q_{block} - Q_{bwc} - Q_{swc} - Q_{alc} - Q_{airc} \tag{16}$$

which can be written as:

$$P_{BW} = Q_{bwh} - Q_{bwc} = \alpha_{teg} I_{bw} T_{bwh} + K_{TE} \Delta T_{bw} - \frac{1}{2} R_{TE} I_{bw}^2 - (\alpha_{teg} I_{bw} T_{bwc} + K_{TE} \Delta T_{bw} - \frac{1}{2} R_{TE} I_{bw}^2) \tag{17}$$

$$P_{SW} = Q_{swh} - Q_{swc} = \alpha_{teg} I_{sw} T_{swh} + K_{TE} \Delta T_{sw} - \frac{1}{2} R_{TE} I_{sw}^2 - (\alpha_{teg} I_{sw} T_{swc} + K_{TE} \Delta T_{sw} - \frac{1}{2} R_{TE} I_{sw}^2) \tag{18}$$

$$P_{AL} = \alpha_{teg} I_{al} T_{alh} + K_{TE} \Delta T_{al} - \frac{1}{2} R_{TE} I_{al}^2 - \frac{(T_{alc} - T_{flow-al})}{R_{thermal,al} + R_{thermal,teg}} = \alpha_{teg} I_{al} (T_{alh} - T_{alc}) - R_{TE} I_{al}^2 \quad (19)$$

$$P_{AIR} = \alpha_{teg} I_{air} T_{airh} + K_{TE} \Delta T_{air} - \frac{1}{2} R_{TE} I_{air}^2 - \frac{(T_{ac} - T_{flow})}{R_{thermal,teg}} = \alpha_{teg} I_{air} (T_{aith} - T_{ac}) - R_{TE} I_{air}^2 \quad (20)$$

where P_{BW}, P_{SW}, P_{AL}, and P_{AIR} are the output power of the thermoelectric module with a large-channel water-cooling radiator, a small-channel water cooling radiator, an aluminium air-cooling radiator and a direct air-cooling structure, respectively, and R_{TE} is the electrical resistance of the thermoelectric module.

As shown in Figure 1A,B, Figure 2A,B, the solar thermoelectric power generator in this paper includes thermoelectric cooling structures (containing three different cooling radiators and a direct air cooling structure), a solar heat transfer pipe, four thermoelectric power generators, a set of water pumps with transparent hoses, solar panels, a water tank, a set of gravity-assisted heat pipes, a thermally conductive copper block, and silica insulation material (placed inside the black surfaces shown in Figure 2B.

The different cooling radiators are a large-channel water-cooling radiator with a channel diameter of 10 mm and external size of 40 × 40 × 12 mm, which is shown in Figure 2A and (b) and (e) in Figure 2B; a small-channel water-cooling radiator with a channel diameter of 2 mm and external size of 40 × 40 × 2.5 mm, which is shown in Figure 2A and (c) and (f) in Figure 2B; and an aluminium air-cooling radiator, which is shown in Figure 2A and (d) in Figure 2B and has an external size of 40 × 40 × 15 mm. These three cooling radiators are tightly placed close to the cold side of the thermoelectric power generator (shown in Figure 2A,B, and this placement contributes to the improvement in the cooling effects of the solar thermoelectric power generator. Both the large- and small-channel water-cooling radiators are connected to water pumps placed in the water tank by different types of transparent hoses, which are shown in (e) and (f) in Figure 2B. The water pumps in the water tank are driven by solar panels, which harvest energy from the outside sunshine as a power source and then provide an output power of 3 W. When the solar panels are exposed to sunlight, the energy begins to be collected and stored, and this energy is then transferred to the water pumps to operate the pumps. When the water pumps operate in stable conditions, the cooling water starts its journey from the water tank shown in Figure 1A to the channels of the large- and small-channel water-cooling radiators. As a result, the cooling water in the channels removes heat from the cold side of the thermoelectric power generator, and this process further improves the output characteristics of the solar thermoelectric power generator.

The length, outer diameter and inside diameter of the solar heat transfer pipe are 1800 mm, 58 mm and 48 mm, respectively, and the internal space of this pipe is embedded in a gravity-assisted heat pipe. The top of the gravity-assisted heat pipe is inserted into a thermally conductive copper block, whose four outside surfaces fit closely with the hot sides of the four thermoelectric modules. Each thermoelectric module is a commercial GM-200-127-14-16 from European Thermodynamics. The output parameters are effectively measured using a series of K-type thermocouples (Thermometers TT-K-30-SLE, Omega, United States), Fluke F15/F17B+ professional digital multimeter measuring tools, CEM (SHENZHEN EVERBEST MACHINERY INDUSTRY CO. LTD.) DT-612 dual-channel thermometer surface thermometers, CEM DT-610B single-channel digital contact thermometers, and CEM DT-8808 Handheld Liquid Crystal Display Illuminance Digital LUX Light Meters. A variable load (ZX-92A from the Shanghai Zheng Yang Instrument Factory) is selected to test the output performance of the device under different load environments. A DC1582 boost chip manufactured by Linear Technology is used to adjust the output parameters of the device to meet the energy supply needs of different types of low-power wireless sensors.

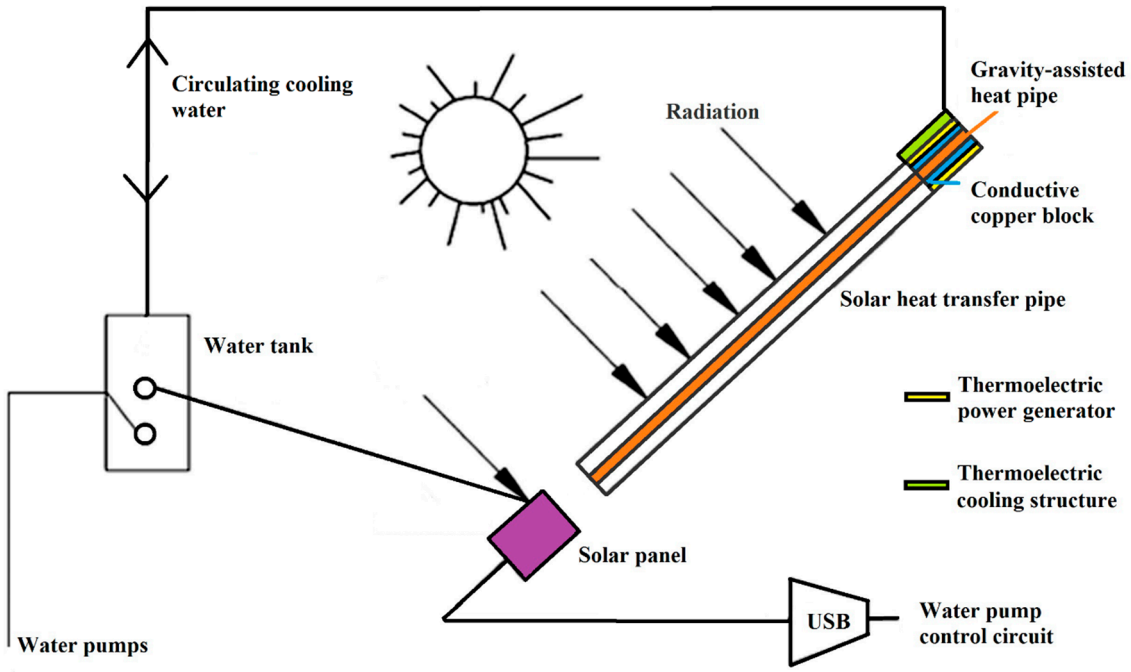

(**A**)

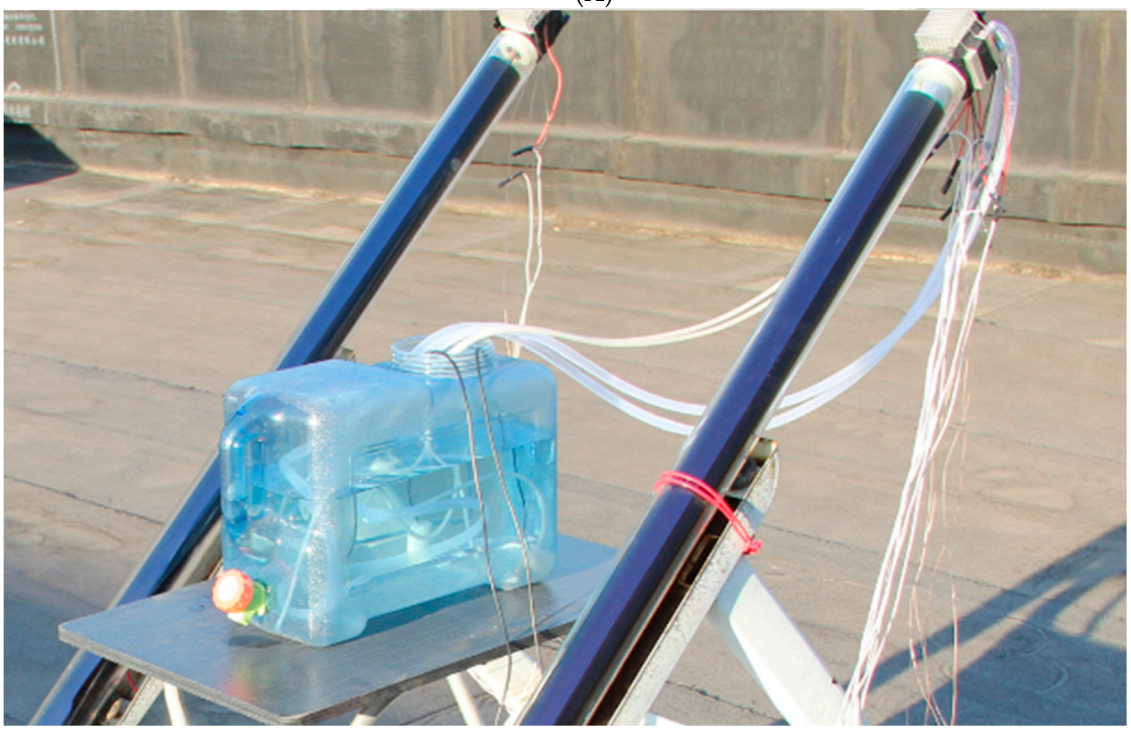

(**B**)

Figure 1. Solar thermoelectric power-generation device: (**A**) schematic diagram; (**B**) experimental rig.

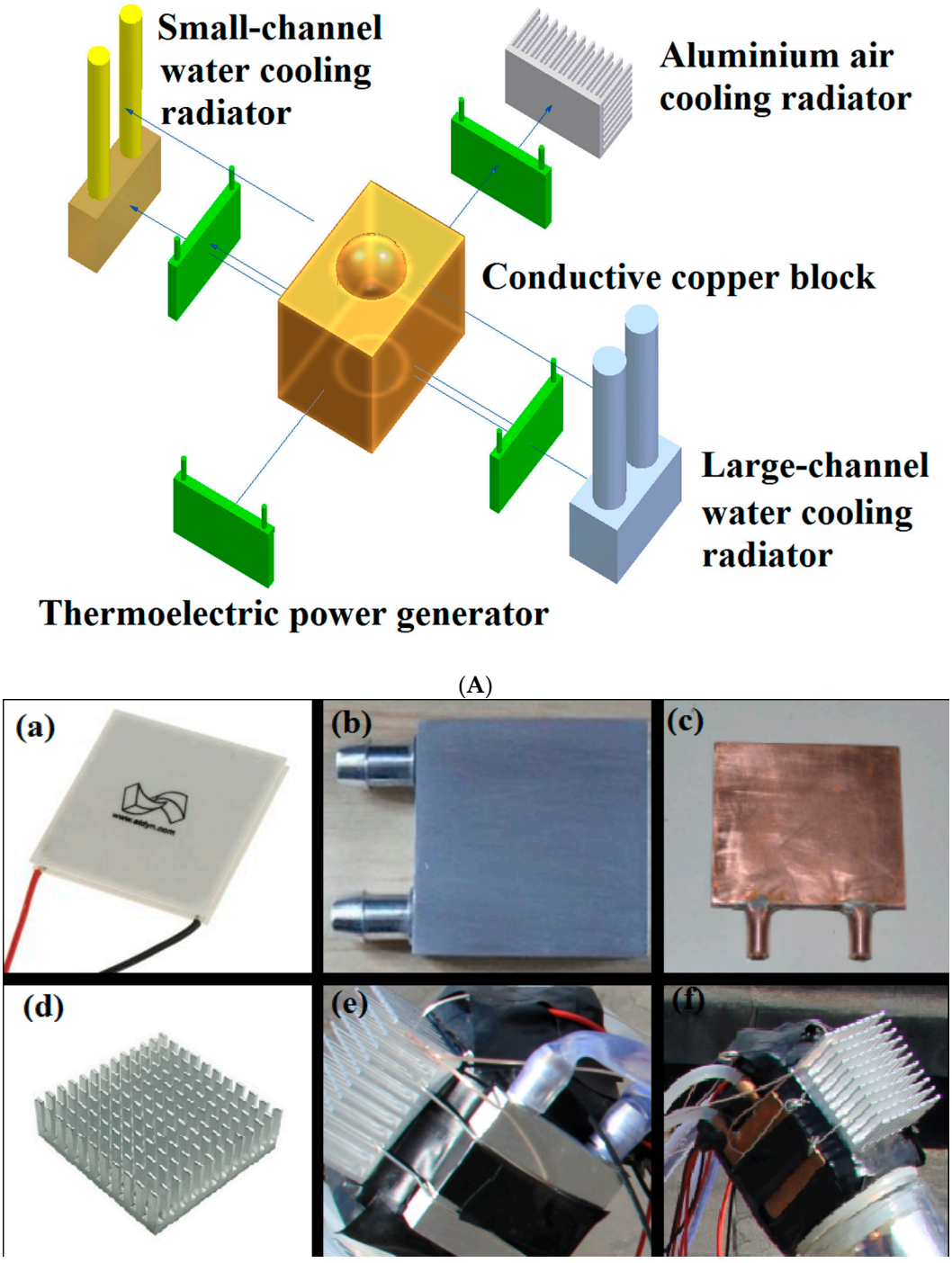

Figure 2. Cooling radiators of the device. (**A**) Schematic diagram; (**B**): (a) thermoelectric power generation module: GM-200-127-14-16; (b) a large-channel water-cooling radiator; (c) a small-channel water-cooling radiator; (d) an aluminium air-cooling radiator; (e) a picture of a large-channel water-cooling radiator and an aluminium air-cooling radiator installed in the system; (f) a picture of a small-channel water-cooling radiator and an aluminium air-cooling radiator installed in the system.

When sunlight irradiates the solar heat transfer pipe, its interior and exterior surface temperatures rise rapidly, and the heat is collected and transferred to the gravity-assisted heat pipe. The gravity-assisted heat pipe transfers heat to the thermally conductive copper block, which then transfers heat to the hot sides of the thermoelectric modules, making the hot-side temperatures

rise sharply. The heat from the hot end is transferred to the cold end through a thermoelectric power generator. As the heat accumulates at the cold side, the temperature of the radiator rises. With the normal work of the efficient cooling structure, the temperatures of the cold sides of the thermoelectric modules are far lower than the temperature of the radiator, resulting in heat convection due to the large temperature differences. Cooling water flows rapidly in the channels of the large- and small-channel water cooling radiators, sharply reducing their temperatures. Additionally, air blows on the aluminium radiator, rapidly decreasing the temperature of the radiator as well as that of the cold end. To better show the cooling effects of the cooling modes, a thermoelectric module tightly placed at the outside surface of the thermally conductive copper block is exposed directly to air without other cooling structures, representing a matched group and the simplest cooling mode. Selectively, an external energy conversion module, such as a DC1582 from Linear Technology, can be chosen to improve the voltage when the thermoelectric voltage reaches the start voltage of the electrical energy collection module, and this module provides a convenient means for collecting and supplying power for low-power loads such as wireless sensors in environmental conditions.

3. Results

The experiments on the concentrated solar thermoelectric power generation system mainly include two parts, which are output parameter tests for the thermoelectric module with a large-channel water cooling radiator under various load resistances shown in Figures 3–7 and continuous output tests for the thermoelectric modules with four different cooling modes shown in Figures 8–11 under a state of regular illumination from 3.14×10^4 lx to 10.04×10^4 lx, with one TEG module in one mode. The first experiment studies the change trends of the output current, output voltage of the load resistance, output power and thermoelectric efficiency of the thermoelectric module with a large-channel water cooling radiator in the case of a gradual increase in load resistance when the temperatures of the hot and cold sides of the thermoelectric module vary within relatively stable small ranges. The second experiment concentrates on the continuous working status of the thermoelectric modules with the four cooling modes, where the output parameters of the four cooling modes are discussed and analysed to provide a reference for a single application or combinations of cooling modes in different cooling circumstances to match the complex requirements of wireless sensors, electronic modules, and other similar loads.

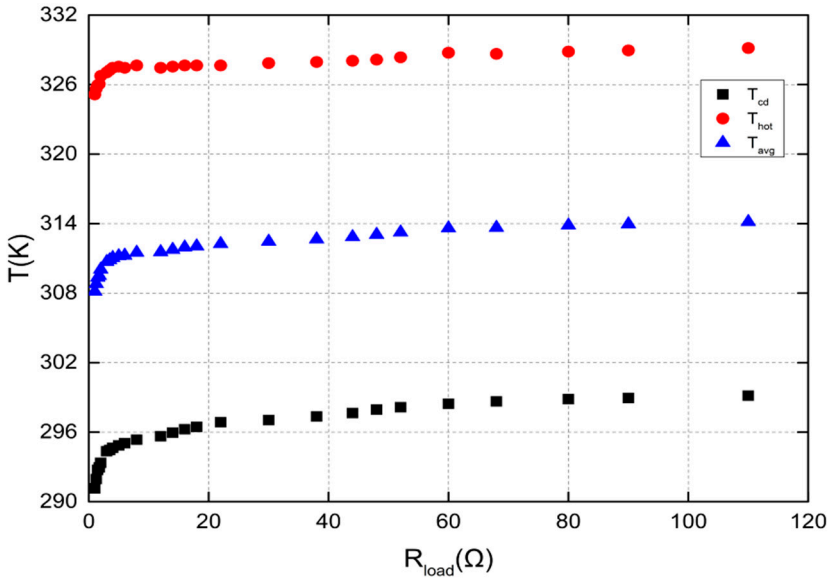

Figure 3. Change trends of T_{hot}, T_{cd} and T_{avg} with the load resistance.

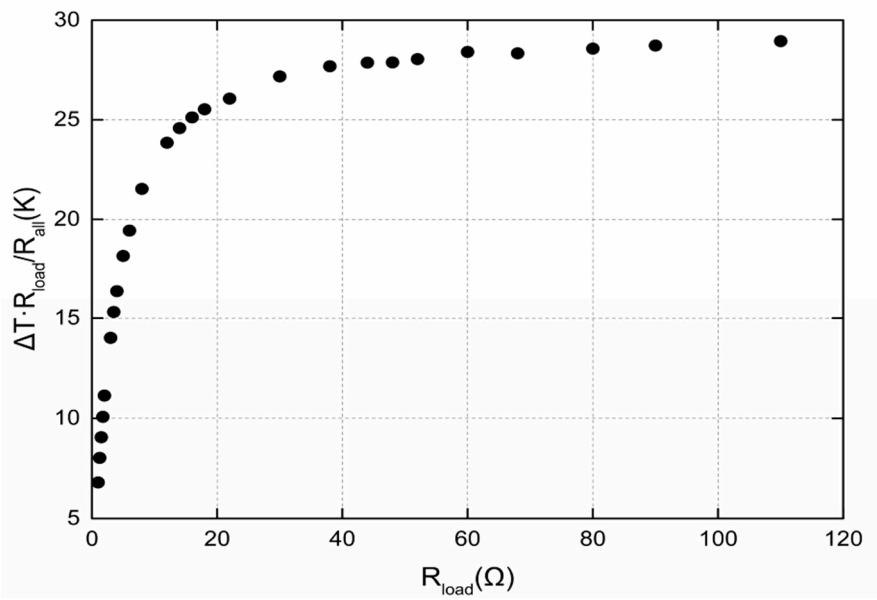

Figure 4. Changing tendency of $\Delta T R_{load}/R_{all}$ on the load resistance.

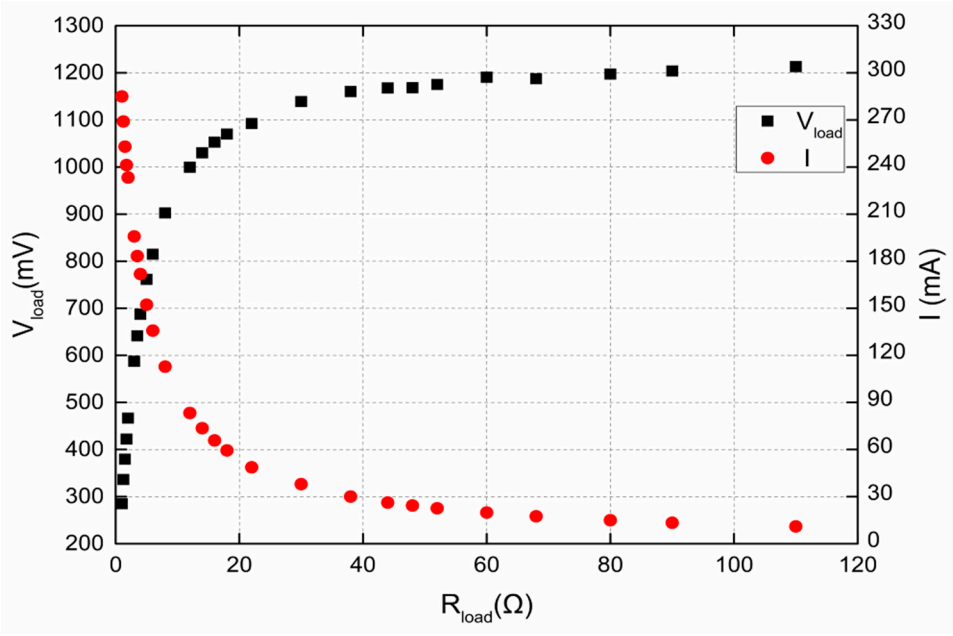

Figure 5. Change trends of V_{load} and I with the load resistance.

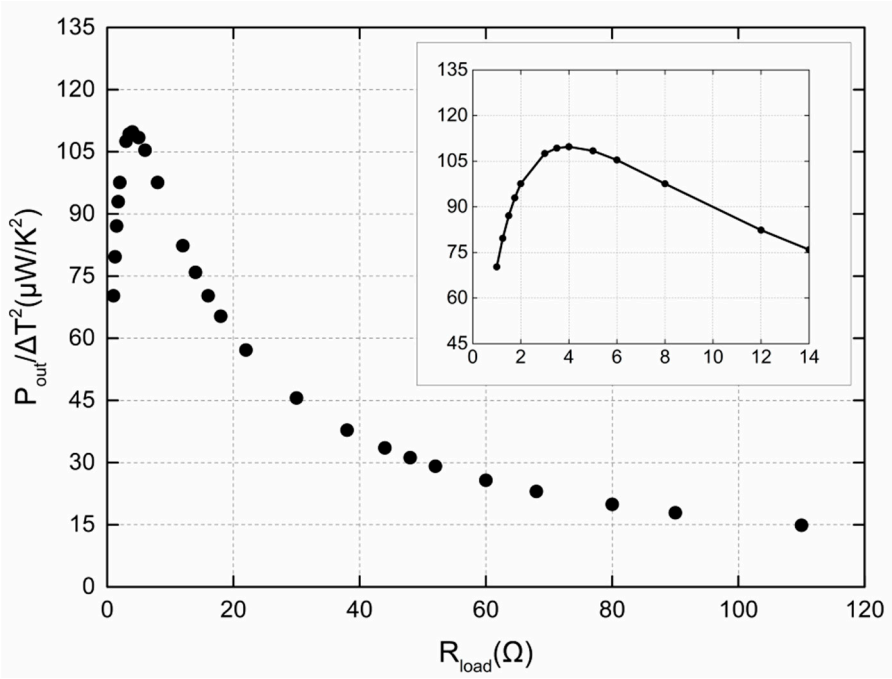

Figure 6. Changes in P_{out} normalized by ΔT^2 as the load resistance changes. Inset: detailed view close to the maximum.

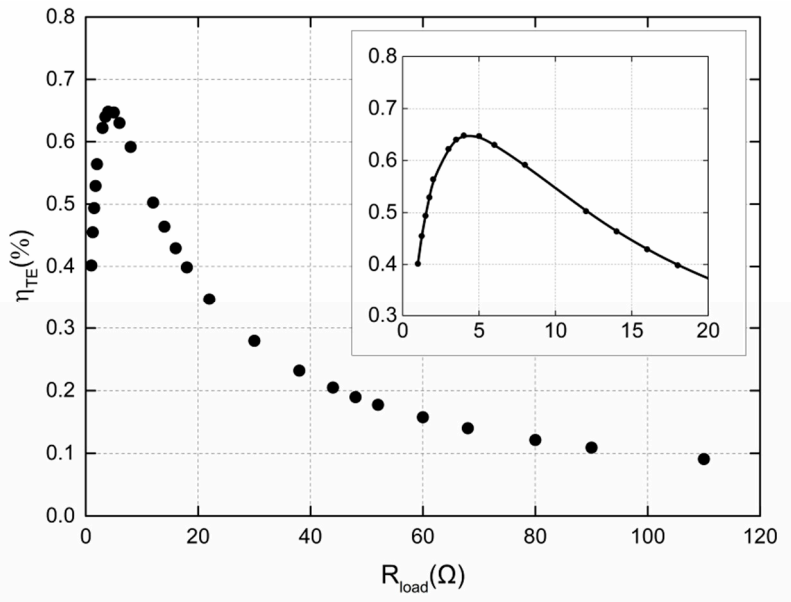

Figure 7. Changes in η_{TE} as the load resistance changes. Inset: detailed view close to the maximum.

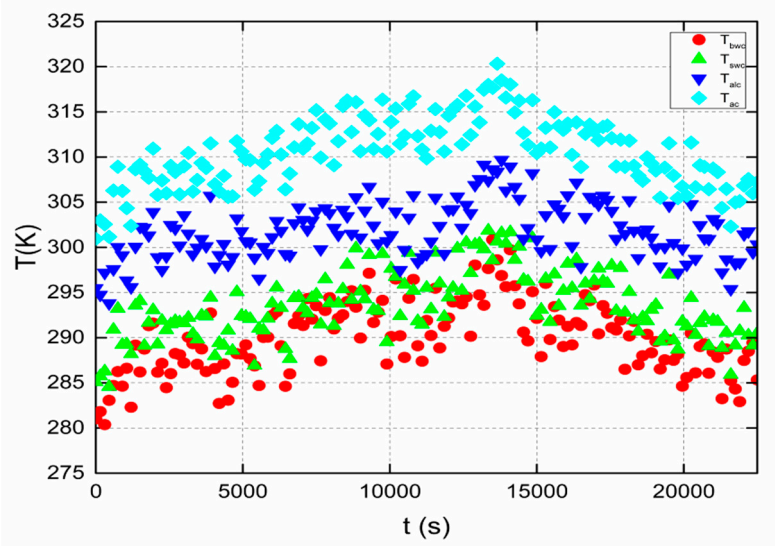

Figure 8. Change trends of T_{bwc}, T_{swc}, T_{alc} and T_{ac} over time during the experiment with changing temperature.

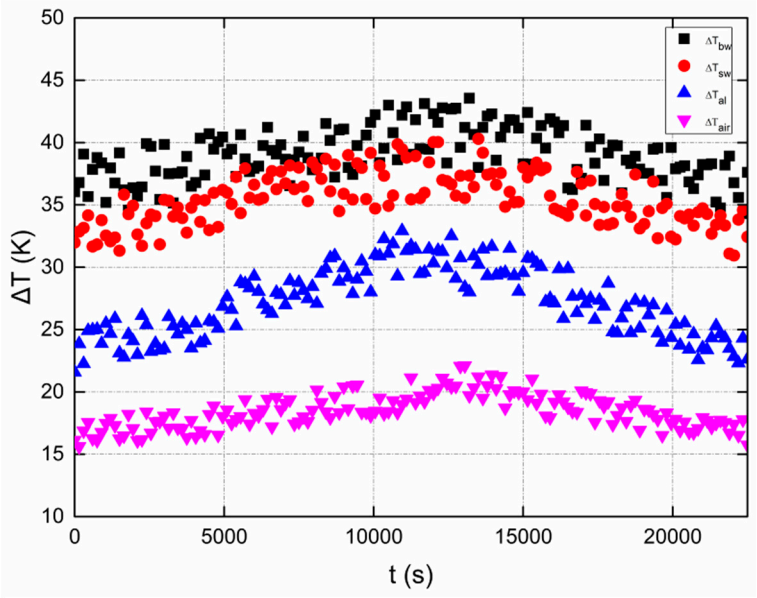

Figure 9. Change trends of ΔT_{bw}, ΔT_{sw}, ΔT_{al}, and ΔT_{air} over time during the experiment with changing temperature.

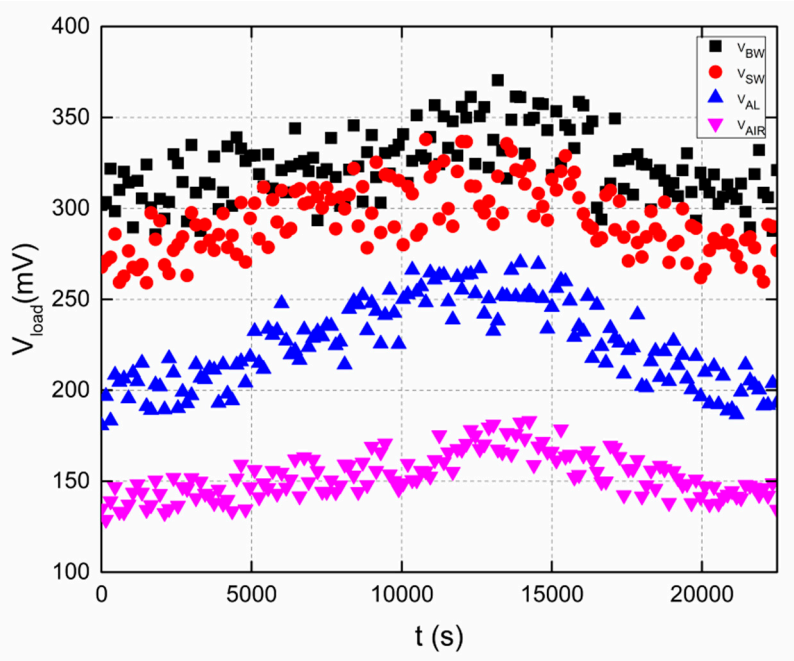

Figure 10. Change trends of V_{BW}, V_{SW}, V_{AL}, and V_{AIR} over time during the experiment with changing temperature.

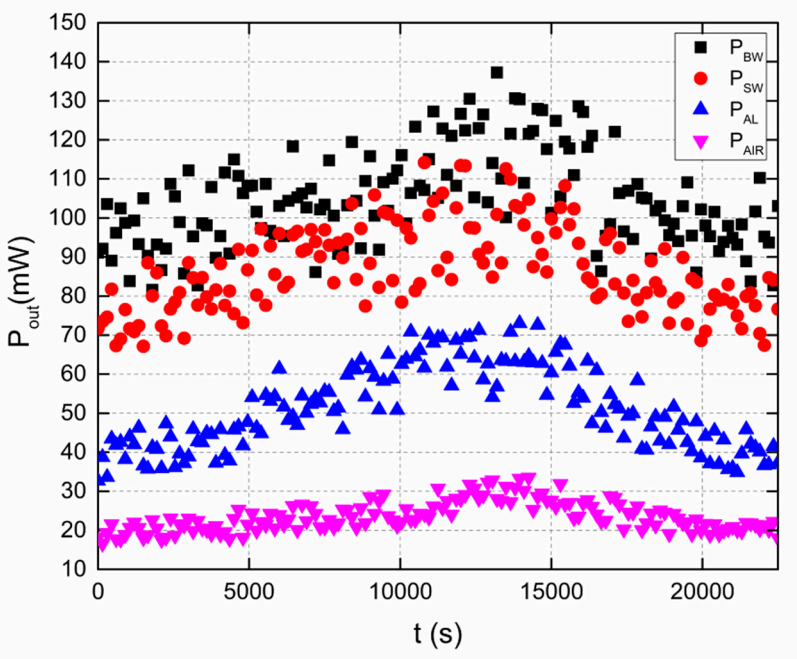

Figure 11. Change trends of P_{BW}, P_{SW}, P_{AL}, and P_{AIR} over time during the experiment with changing temperature.

As shown in Figure 3, when the load resistance changes from 1 ohm to 110 ohm, the temperatures of the cold sides of the thermoelectric modules (shown in Figure 3 as T_{cd}) vary from 291.2 K to 299.2 K, the temperatures of the hot sides of the thermoelectric modules (shown in Figure 3 as T_{hot}) vary from 325.2 K to 329.2 K, and the average temperatures between the hot and cold sides of the thermoelectric modules (shown in Figure 3 as T_{avg}) vary from 308.2 K to 314.2 K. Considering that the electrical resistance of a thermoelectric module is 4 ohm, the temperature data are centrally tested when the load resistance changes from 1 ohm to 10 ohm. As the load resistance increases, the energy collected by the concentrated solar thermoelectric power-generation system accumulates, making the heat

exchange between the thermoelectric module and the outside environment gradually become stable. When the load resistance is larger than 60 ohm, the temperature changes on the hot and cold sides of the thermoelectric module are no longer obvious, indicating that heat exchange stability has been reached.

Figures 4 and 5 show the change trends of $\Delta T R_{load}/R_{all}$, the output voltage and the output current of the thermoelectric module with a large-channel water cooling radiator under various load resistances. Here, Rall means the whole resistance of the device, comprising the load resistance and inner resistance of the thermoelectric power generator. With an increase in the load resistance, the values of $\Delta T R_{load}/R_{all}$ sharply increase, leading to a substantial growth in the output voltage. The reason for this increase is that the ratio of the load resistance to the total resistance gradually increases when the load resistance changes from 1 ohm to 110 ohm, but the electrical resistance of the thermoelectric module remains at 4 ohm. Moreover, it is clear that as the load resistance increasingly approaches the total resistance of the system, the growth rate of $\Delta T R_{load}/R_{all}$ gradually decreases, resulting in a decreasing growth rate of the output voltage. According to Ohm's law, it is clear that the change trend of the output current is inversely proportional to that of the total resistance, and this effect is obviously observed in Figure 5. The maximum output voltage is 1213.2 mV when the load resistance is 110 ohm, which suggests that the impact of the ratio of the load resistance on the output voltage is significant.

The output power and thermoelectric efficiency of the thermoelectric module are shown in Figures 6 and 7. The peak value of $P_{out}/\Delta T^2$ is 109.78 μW/K^2 when the load resistance reaches 4 ohm, which is equal to the value of the electrical resistance of the thermoelectric module. The reason for this is that the largest output power occurs when the load resistance is the same as the inner resistance of the system, which is the electrical resistance of the thermoelectric module in this experiment. This result provides an efficient solution to obtain the largest output power when the concentrated solar thermoelectric power-generation system is used to power various loads. However, this solution is hard to realize because of the minor load resistances of low-power loads that are no more than one ohm. As a result, the values of $P_{out}/\Delta T^2$ and the thermoelectric efficiency are important when the load resistance is close to one ohm. In this experiment, when the load resistance is one ohm, the values of $P_{out}/\Delta T^2$ and the thermoelectric efficiency are 70.3 μW/K^2 and 0.4%, respectively, which provide a reference for the application of the system when the load is approximately one ohm.

The continuous working test experiment of the thermoelectric modules with the four cooling modes was carried out in outdoor conditions in Beijing. The value of the load resistance was chosen to be one ohm to test the output performance of the concentrated solar thermoelectric power-generation system under low-power load conditions. The output parameters were acquired and are shown in Figures 8–11, which present the continuous change trends of the temperatures of the cold sides of the thermoelectric modules (shown in Figure 8 as T_{lwc}, T_{swc}, T_{alc}, and T_{ac}, which are the temperatures of the cold sides of the thermoelectric modules in large-channel water-cooling mode, small-channel water cooling mode, aluminium radiator cooling mode and air cooling mode, respectively), the temperature differences between the hot and cold sides of the thermoelectric modules, the output voltage and the output power. The peak values of the temperature difference between the hot and cold sides of the thermoelectric modules, the output voltage and the output power are 43.6 K, 370.4 mV and 137.2 mW, respectively, which were obtained when the experiment had been carried out for three hours and 40 min.

4. Discussion

The output power shown in Figure 6 is closely related to the output current of the thermoelectric module with a large-channel water-cooling radiator under various load resistances, as shown in Figure 5. As shown in Equations (7), (11) and (17), the output current of the thermoelectric module with a large-channel water-cooling radiator has a significant impact on the energy reaching the hot side of the thermoelectric module with a large-channel water-cooling radiator, the energy acquired at the cold side of the thermoelectric module with a large-channel water-cooling radiator and the output power of the thermoelectric module with a large-channel water-cooling radiator. On the one hand, as the output

current of the thermoelectric module with a large-channel water-cooling radiator increases, the values of $\alpha_{teg} I_{bw} T_{bwh}$ and $\alpha_{teg} I_{bw} T_{bwc}$ increase, which contributes to increases in the energy reaching the hot and cold sides of the thermoelectric module with a large-channel water-cooling radiator and the output power. On the other hand, as the aforementioned output current increases, the value of $-0.5 R_{te} {I_{bw}}^2$ increases, which reduces the amount of energy reaching the hot and cold sides of the thermoelectric module with a large-channel water-cooling radiator and the output power. The change trend of the output power shown in Figure 6 is the result of the combined effect of the above two change trends. When the output current of the thermoelectric module with a large-channel water-cooling radiator shown in Figure 5 is less than 150 mA, the output power shown in Figure 6 continues to increase. During this time, the changes in $\alpha_{teg} I_{bw} T_{bwh}$ and $\alpha_{teg} I_{bw} T_{bwc}$ have a significant effect on the final output power. The decrease in the output power shown in Figure 6 starts when the output current shown in Figure 5 is greater than 150 mA, as the change in $-0.5 R_{te} {I_{bw}}^2$ has a more important effect on the final output power.

The thermoelectric efficiency of the thermoelectric module η_{TE} shown in Figure 7 changes from 0.40% to 0.65% when the load resistance varies from 0 to 180 ohm. According to thermoelectric conversion theory and calculations of thermoelectric efficiency in previous literature [3,4], the thermoelectric efficiency is closely related to the temperatures of the hot and cold sides of the thermoelectric module (shown in Figure 3 as T_{hot} and T_{cd}, respectively), the thermoelectric figure of merit, and the ratio of the load resistance to the internal resistance of the thermoelectric power generator. The thermoelectric figure of merit of a GM-200-127-14-16 from European Thermodynamics is 9.045×10^{-4} (1/K). Therefore, the change trend of the thermoelectric efficiency of the thermoelectric module η_{TE} is affected by key parameters such as Thot and T_{cd} and the ratio of the load resistance to the internal resistance of the thermoelectric power generator. The change in the ratio of the load resistance to the internal resistance can be calculated accurately, as shown in Figure 7, when the load resistance varies from 0 to 180 ohm and the internal resistance remains unchanged at 4 ohm. The key parameters T_{hot} and T_{cd} are affected by different factors. T_{hot} is affected by the energy reaching the hot side of the thermoelectric module with a large-channel water-cooling radiator and can be calculated by Equation (7). When the light intensity increases, the energy that reaches the hot side of the thermoelectric module increases, resulting in a larger value of T_{hot}. The value of T_{cd} depends on the cooling efficiency of the cooling structure located at the cold side of the thermoelectric module. Both the values of T_{hot} and T_{cd} are able to be directly acquired through thermometers, making the calculation of thermoelectric efficiency more accurate. The maximum value of the thermoelectric efficiency is 0.65% during the experiment and can be further improved with a better light intensity or cooling method in future studies.

The output parameters of the four different cooling modes deserve further analysis. According to Figure 8, which shows the exact temperature data of T_{bwc}, T_{swc}, T_{alc} and T_{ac}, it is obvious that the values of the four parameters ordered from small to large are T_{bwc}, T_{swc}, T_{alc} and T_{ac}, which means that the cooling performance of the four parameters ranging from strong to weak follows the order T_{bwc}, T_{swc}, T_{alc} and T_{ac}. The reason for this phenomenon is that with a stable flow speed of cooling water, the energy transferred by the cooling water is much greater than that transferred by air blowing either on the aluminium radiator or directly on the cold side of the thermoelectric module. For the large-channel and small-channel water-cooling modes, it is easy to determine that during the same time period, the large-channel water-cooling structure carries more energy than the small-channel water cooling structure because of its larger water flow. When the cooling performance of aluminium radiator cooling and that of air cooling are compared, the key parameter is the cooling area of the cooling surface. With a larger area of the cooling surface, the performance of aluminium radiator cooling is better than that of air cooling. The temperature difference values ΔT_{bw}, ΔT_{sw}, ΔT_{al}, and ΔT_{air} are shown in Figure 9, and these values vary from 15 K to 45 K. The values of the four parameters ordered from large to small are ΔT_{bw}, ΔT_{sw}, ΔT_{al}, and ΔT_{air}, which means that the cooling performance of the four parameters ranging from strong to weak follows the order ΔT_{bw}, ΔT_{sw}, ΔT_{al}, and ΔT_{air}. The temperature difference

values for water cooling are more than 10 K greater than those for aluminium radiator cooling, and this result indisputably reveals the strong cooling effect of water cooling.

As shown in Figures 10 and 11, the exact values of V_{BW}, V_{SW}, V_{AL}, and V_{AIR} and those of P_{BW}, P_{SW}, P_{AL}, and P_{AIR} are obtained, respectively. As a whole, it is obvious that the values of the first four parameters ordered from large to small are V_{BW}, V_{SW}, V_{AL}, and V_{AIR}, which means that the cooling performance of the four parameters ranging from strong to weak follows the order V_{BW}, V_{SW}, V_{AL}, and V_{AIR}. The reason for this result is similar to the reason discussed for the exact temperature data. As shown in Figure 10, the largest values of V_{BW}, V_{SW}, V_{AL}, and V_{AIR} are 370.4, 337.9, 270.2 and 183.1 mV, respectively. These values are acquired when the load resistance of the solar thermoelectric power generation system is 1 ohm, which is close to the exact value of low-power loads such as wireless sensors. As the inner resistance of the thermoelectric power generator is 4 ohm, it is easy to increase the value of the output voltage when a larger load resistance is chosen.

As shown in Figure 11, the largest values of P_{BW}, P_{SW}, P_{AL}, and P_{AIR} are 137.2, 114.2, 73.0 and 33.5 mW, respectively. Under the same constant pumping power condition, the cooling output power performance of the large-channel water cooling is better than that of the small-channel water cooling because of its larger channel diameter, which results in a larger heat exchange area and improves the heat exchange efficiency between the cold side of the thermoelectric module and the cooling structures. However, as the pump power is constant, the volume of water sprayed by the pump is a fixed value, which means that the larger the heat exchange area, the slower the fluid shifting speed will be. At this point, choosing an appropriate heat exchange area and fluid shifting speed is critical for achieving satisfactory cooling performance. Taking the values of the output voltage and output power as a reference, large-channel water cooling exhibits better performance than small-channel water cooling in the cooling process of the solar thermoelectric power generator, showing a 20.14% increase in output power and a 9.62% increase in output voltage. For the cooling output power performance of aluminium radiator cooling and air cooling, the heat exchange mode is natural convection heat transfer of air for both, and the key parameter of cooling is the heat exchange area. It is clear that aluminium radiator cooling has a larger heat exchange area than air cooling and, as a result, when the sizes of the air flow rates between the cold side of the thermoelectric module and the cooling structures are similar, the larger the heat exchange area, the better the cooling performance that will be achieved. Taking the values of the output voltage and output power as a reference, aluminium radiator cooling exhibits better performance than air cooling in the cooling process of the solar thermoelectric power generator, showing a 117.91% increase in output power and a 47.57% increase in output voltage, and these results are clearly and intuitively reflected in Figures 10 and 11.

5. Conclusions

In this work, a new solar thermoelectric conversion device based on an all-glass solar heat transfer pipe and gravity-assisted heat pipe with recycling air cooling and water cooling circuits is designed. With different cooling modes, such as large-channel water cooling, small-channel water cooling, aluminium radiator cooling and air cooling, the device can realize four separate output modes and multiple composite output modes. This device has practical significance for meeting different load power requirements, such as wireless sensors, electronics, and other loads. When the system is installed with only a large-channel water cooling radiator, the maximum output voltage is 1213.2 mV when the load resistance is 110 ohm, and the peak value of the thermoelectric efficiency of the thermoelectric module $P_{out}/\Delta T^2$ is 109.78 $\mu W/K^2$ when the load resistance reaches 4 ohm. Under a state of regular illumination from 3.14×10^4 lx to 10.04×10^4 lx, with one GM-200-127-14-16 TEG module from European Thermodynamics in one mode and 1 ohm load resistance, the peak output voltage and power values of the device with large-channel water cooling, small-channel water cooling, aluminium radiator-cooling and air-cooling modes are 370.7 mV, 337.9 mV, 270.2 mV, and 183.1 mV and 137.2 mW, 114.2 mW, 73.0 mW, and 33.5 mW, respectively. The results show that large-channel water cooling exhibits a 20.14% increase in output power and a 9.62% increase in output voltage compared

with small-channel water cooling under the same flow of the water pump. Aluminium radiator cooling exhibits a 117.91% increase in output power and a 47.57% increase in output voltage compared with air cooling under the same air flow. These results provide evidence of specific output performance levels and a combination basis for multiple composite output modes to meet different load power requirements, such as wireless sensors, electronics, and other loads. All parameters are continuously measured in outdoor circumstances without man-made power supported by urban electricity, and this aspect contributes to the development and utilization of green clean energy. The cost of the system is approximately $200, indicating the system's cost-effectiveness and high availability when it is applied in a stable process. Furthermore, the output energy of the system can be collected, stored, and then output or directly applied to a load to provide an energy supply through a boost and voltage stabilization circuit such as a DC1582 from Linear Technology. The energy supply of the above structure is completely obtained from the natural environment, and this aspect provides a high reference value for the cross-research of natural environment energy utilization and thermoelectric energy-conversion technology.

Author Contributions: All authors contributed to the paper. W.L., provided guidance, supervision, and revised the paper; Z.Z., designed the research, conceived the idea of the study, and wrote the paper; Z.Z. and Y.W., performed the experiment and discussed experimental results; Z.Z. and D.X., discussed the experimental results and revised the paper. All authors have read and agreed to the published version of the manuscript.

Funding: The authors gratefully acknowledge the financial support from the National Science Foundation of China (31670716), the China Postdoctoral Science Special Foundation (2016T90044) and the China Postdoctoral Science Foundation (2015M570945).

Conflicts of Interest: The authors declare no conflict of interest.

References

1. Zhao, L.D.; Tan, G.J.; Hao, S.Q.; He, J.Q.; Pei, Y.L.; Chi, H.; Wang, H.; Gong, S.; Xu, H.; Dravid, V.P.; et al. Ultrahigh power factor and thermoelectric performance in hole-doped single-crystal SnSe. *Science* **2016**, *351*, 141–144. [CrossRef] [PubMed]
2. He, J.; Tritt, T.M. Advances in thermoelectric materials research: Looking back and moving forward. *Science* **2017**, *357*, eak9997. [CrossRef]
3. Zhang, Z.; Li, W.B.; Kan, J.M. Behavior of a thermoelectric power generation device based on solar irradiation and the earth's surface-air temperature difference. *Energy Convers. Manag.* **2015**, *97*, 178–187. [CrossRef]
4. Zhang, Z.; Li, W.B.; Kan, J.M.; Xu, D.C. Theoretical and experimental analysis of a solar thermoelectric power generation device based on gravity-assisted heat pipes and solar irradiation. *Energy Convers. Manag.* **2016**, *127*, 301–311. [CrossRef]
5. Demir, M.E.; Dincer, I. Development of an integrated hybrid solar thermal power system with thermoelectric generator for desalination and power production. *Desalination* **2017**, *404*, 59–71. [CrossRef]
6. Karthick, K.; Suresh, S.; Joy, G.C.; Dhanuskodi, R. Experimental investigation of solar reversible power generation in Thermoelectric Generator (TEG) using thermal energy storage. *Energy Sustain. Dev.* **2019**, *48*, 107–114. [CrossRef]
7. Kumar, A.; Singh, K.; Verma, S.; Das, R. Inverse prediction and optimization analysis of a solar pond powering a thermoelectric generator. *Sol. Energy* **2018**, *169*, 658–672. [CrossRef]
8. Sathiyanathan, M.; Jaganathan, S.; Josephine, R.L. Design and Analysis of Universal Power Converter for Hybrid Solar and Thermoelectric Generators. *J. Power Electron.* **2019**, *19*, 220–233.
9. Zhang, X.F.; Gao, W.Q.; Su, X.W.; Wang, F.L.; Liu, B.S.; Wang, J.J.; Liu, H.; Sang, Y. Conversion of solar power to chemical energy based on carbon nanoparticle modified photo-thermoelectric generator and electrochemical water splitting system. *Nano Energy* **2018**, *48*, 481–488. [CrossRef]
10. Zhu, W.; Deng, Y.; Gao, M.; Wang, Y.; Cui, J.L.; Gao, H.L. Thin-film solar thermoelectric generator with enhanced power output: Integrated optimization design to obtain directional heat flow. *Energy* **2015**, *89*, 106–117. [CrossRef]
11. Kwan, T.H.; Wu, X.F. Power and mass optimization of the hybrid solar panel and thermoelectric generators. *Appl. Energy* **2016**, *165*, 297–307. [CrossRef]

12. Marandi, O.F.; Ameri, M.; Adelshahian, B. The experimental investigation of a hybrid photovoltaic-thermoelectric power generator solar cavity-receiver. *Sol. Energy* **2018**, *161*, 38–46. [CrossRef]
13. Singh, S.; Ibeagwu, O.I.; Lamba, R. Thermodynamic evaluation of irreversibility and optimum performance of a concentrated PV-TEG cogenerated hybrid system. *Sol. Energy* **2018**, *170*, 896–905. [CrossRef]
14. Lekbir, A.; Meddad, M.; Eddiai, A.; Benhadouga, S.; Khenfer, R. Higher-efficiency for combined photovoltaic-thermoelectric solar power generation. *Int. J. Green Energy* **2019**, *16*, 371–377. [CrossRef]
15. Zhu, W.; Deng, Y.; Wang, Y.; Shen, S.F.; Gulfam, R. High-performance photovoltaic-thermoelectric hybrid power generation system with optimized thermal management. *Energy* **2016**, *100*, 91–101. [CrossRef]
16. Karimov, K.S.; Ahmad, Z. A two-stage solar collector using a non-tracking conical concentrator and a glass lens for PV-TEG hybrid system. *Appl. Phys. A* **2018**, *124*, 857. [CrossRef]
17. Rodrigo, P.M.; Valera, A.; Fernandez, E.F.; Almonacid, F.M. Performance and ecnomic limits of passively cooled hybrid thermoelectric generator-concentrator photovoltaic modules. *Appl. Energy* **2019**, *238*, 1150–1162. [CrossRef]
18. Maolikul, S.; Kiatgamolchai, S.; Chavarnakul, T. Low-Power Energy Harvesting of Thermoelectric Battery Charger with Step-Up DC-DC Converter: Applicable Case Study for Personal Electronic Gadgets. *J. Energy Eng.* **2017**, *143*, 05017001. [CrossRef]
19. Chen, W.H.; Liao, C.Y.; Wang, C.C.; Hung, C.I. Evaluation of power generation from thermoelectric cooler at normal and low-temperature cooling conditions. *Energy Sustain. Dev.* **2015**, *25*, 8–16. [CrossRef]
20. Ding, L.C.; Akbarzadeh, A.; Tan, L. A review of power generation with thermoelectric system and its alternative with solar ponds. *Renew. Sustain. Energy Rev.* **2018**, *81*, 799–812. [CrossRef]
21. Ma, M.; Yu, J.L. Experimental study on transient cooling characteristics of a realistic thermoelectric module under a current pulse operation. *Energy Convers. Manag.* **2016**, *126*, 210–216. [CrossRef]
22. Date, A.; Date, A.; Dixon, C.; Akbarzadeh, A. Theoretical and experimental study on heat pipe cooled thermoelectric generators with water heating using concentrated solar thermal energy. *Sol. Energy* **2014**, *105*, 656–668. [CrossRef]